

Small-Molecule Absorber A1094 as a Stable and Fast-Clearing NIR-II Imaging Agent

Yanfang Huang,^[a] Huanhuan Liu,^[a] Xueyuan Chen,^[a] Yunming Zhang,^[a] Xingyang Zhao,^[a, b] Wenchao Huang,^[a] Zhaobiao Mou,^[a] Chao Wang,^[a] Kaiqiang Zhang,^[a] and Zijing Li^{*[a]}

Photoacoustic imaging (PAI) in the second near-infrared window (NIR-II) is conducive to deep-tissue imaging due to small scattering coefficients, but often requires exogenous imaging agents. At present, nanoparticle-based NIR-II imaging agents are mainly used in non-clinical studies, some basic components of which are resistant to metabolism *in vivo*. The aim of this study was to examine the ~600 Da croconaine absorber A1094, absorbing lights around 1094 nm, as a rare, small-molecule NIR-II imaging agent *in vivo*. The clinical translational potential of A1094 injection were systematically revealed, including sufficient solubility and freeness in blood, good anti-interference ability, and favourable pH/oxidation-reduction/metabolic stabilities. After intravenous administration of A1094

injection, PAI of murine ears exhibited comparable capillaries visibility to that of PAI with popular Au nanorods. The contrasts achieved with A1094 and Au nanorods were 1.78 and 1.29 times higher than before administration, in the healthy group, and 3.25 and 1.58 times higher in the inflammation group. Notably, A1094 demonstrated a desired faster liver clearance than Au nanorods. The PAI signal of A1094 was cleared by 74.2% after 3 h, whereas Au nanorods were only cleared by 43.1%. The main metabolic mechanisms of A1094 were identified as N-methylation and lipid hydrolysis by murine liver microsomes *in vitro*. Therefore, A1094 may have promising clinical potential as a stable and fast-clearing NIR-II imaging agent.

Introduction

Photoacoustic (PA) imaging (PAI) is a hybrid biomedical imaging modality that integrates optical excitation and ultrasound detection.^[1,2] The shifting of excitation wavelengths from the first near-infrared window (NIR-I; 700–1000 nm) to the second near-infrared window (NIR-II; 1000–1700 nm) can result in reduced tissue scattering, deeper tissue penetration, minimised background autofluorescence, and improved image fidelity.^[3–5] Due to the insufficiency of the NIR-II PA signal generated by tissues, exogenous contrast agents are often necessary to enhance the contrast and specificity of PAI in large volumes of biological tissues.^[6–8]

Researchers have endeavoured to explore efficient and biocompatible contrast agents for NIR-II PAI. Most of the current contrast agents are inorganic materials, including metal sulphides, such as CuS, Ag₂S, and ZnS,^[9–11] carbon-based nano-absorbers,^[12] and semi-conductor nanocrystals.^[13] However, unfavourable biocompatibility and pharmacokinetics have impeded the clinical application of these materials. In contrast,

organic absorbers are highly attractive, by virtue of their higher biocompatibility, relatively small molecular mass, and rapid clearance from the body.^[3,7] However, due to disadvantages such as low PA signal, poor photostability, and small optical absorption cross sections,^[14] the vast majority of the organic absorbers used as contrast agents must be currently enclosed in liposome polymer matrices to increase absorption efficiency, stability and agent size beyond the renal clearance threshold.^[3,15,16] Liposomes are also prone to oxidation and are sensitive to temperature and pH, so this strategy is still associated with some practical problems. Ideally, optical probes for clinical use should be easily metabolised and should possess excellent optical properties, light stability, and biocompatibility.^[17] Hence, further efforts are necessary to develop small-molecule organic absorbers with sufficient photostability, absorption, NIR-II PA signal generation and favourable pharmacokinetics.^[18,19]

A1094, a ring-open croconaine derivative first synthesised by Tian et. al for use in optical communications, is perhaps the smallest of the few small organic molecules with an absorption wavelength greater than 1000 nm.^[20,21] Its characteristic strong NIR-II absorption peak at 1094 nm with a high molar extinction coefficient ($7.3 \times 10^4 \text{ L mol}^{-1} \text{ cm}^{-1}$) is attributed to its dielectric large π -conjugated structure, which greatly promotes electron resonance and energy transfer.^[22] A1094 is more stable than the traditional long-straight-chain cyanine absorbers *in vitro*, probably due to its short-planar, rigid structure.^[23–25] However, it is not clear yet whether A1094 qualifies as a NIR-II PAI agent, i.e. whether it possesses the stability, safety, and fast clearance *in vivo* which are required of optical probes used for clinical applications. Therefore, we aimed to provide a first comprehen-

[a] Y. Huang, H. Liu, X. Chen, Y. Zhang, X. Zhao, W. Huang, Z. Mou, C. Wang, K. Zhang, Dr. Z. Li
Center for Molecular Imaging and Translational Medicine
State Key Laboratory of Molecular Vaccinology and Molecular Diagnostics
School of Public Health
Xiamen University
Xiamen, Fujian 361102 (China)
E-mail: zijing.li@xmu.edu.cn

[b] X. Zhao
Department of Hepatobiliary Surgery
Zhujiang Hospital, Southern Medical University
Guangzhou, 510280 (China)

Supporting information for this article is available on the WWW under <https://doi.org/10.1002/cmdc.202100125>

sive preclinical evaluation of A1094 and its potential application in basic blood pool imaging.

Results and Discussion

Characterization and physicochemical properties of A1094

The characterization of the deep-purple solid A1094 (yield: 8.3%) by MS, ^1H and ^{13}C NMR is shown in Figures S8, S9 and S10. The UV-Vis-NIR absorption spectra of the same concentration of A1094 in different organic solvents and aqueous solution featured a broad, strong peak with 1094 nm as the middle axis (Figure S1). A1094 possessed the strongest absorption capacity in acetonitrile ($\epsilon = 7.3 \times 10^4 \text{ L} \times \text{mol}^{-1} \times \text{cm}^{-1}$), followed by that in dichloromethane ($\epsilon = 4.7 \times 10^4 \text{ L} \times \text{mol}^{-1} \times \text{cm}^{-1}$) and DMSO ($\epsilon = 3.6 \times 10^4 \text{ L} \times \text{mol}^{-1} \times \text{cm}^{-1}$) (Figure S4), probably due to higher polarity. The absorption capacity in aqueous solution was approximately the same as that in non-protonic solvents such as dichloromethane (Figure S4). The absorption intensity of A1094 was about three times higher than that of the Au nanorods at an equal mass concentration (0.05 mg/mL) (Figure 1j).

By observing the dissolution of solid A1094 and the colour change before and after dissolution (Figure 1i), it was concluded that A1094 was easily soluble in dichloromethane and acetonitrile, soluble in methanol, DMSO and ethanol, and slightly soluble in cyclohexane and n-hexane. It was also soluble in aqueous solution containing 0.25% DMSO, with solubility up to 0.5 mg/mL.

Stability of A1094

In terms of pH stability, the UV-Vis absorption spectra remained almost unchanged in the range of pH 6–8 (Figures 1b, 1c), the physiological pH interval. After the addition of various metal ions, the UV-Vis absorption spectra were nearly consistent with that of the control (Figure 1d). This observation indicated that A1094 injection possessed a strong anti-interference ability in the presence of biologically necessary metal ions. The absorption spectra of A1094 in solutions containing glutathione and H_2O_2 indicated that the endogenous redox species had a negligible effect on the chemical stability of A1094 (Figure 1d). When A1094 was dissolved in FBS, the absorption intensity decreased only slightly over a course of 120 min (Figure 1e). These characteristics indicate that A1094 injection showed

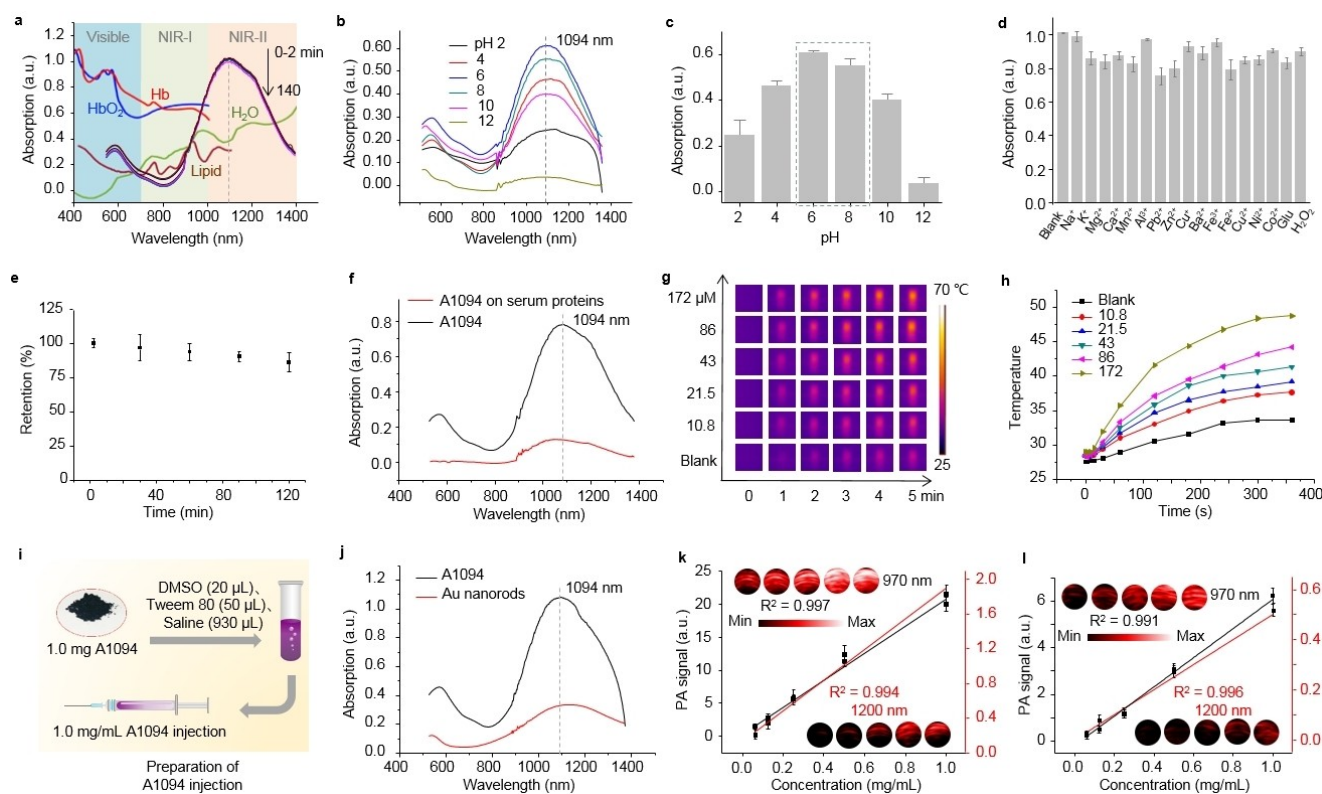


Figure 1. Stabilities, photothermal and photoacoustic properties of small-molecular absorber A1094. (a) Absorption spectra of A1094 over 0–140 min with 10/20 min intervals in an aqueous solution (0.25% DMSO) and absorption spectra of endogenous tissue chromophores in the human body.^[26] (b) Absorption spectrum of A1094 at different pH values. (c) Absorption intensity of A1094 corresponding to (b). (d) Stability of A1094 in the presence of various metal ions and re-dox species. (e) Retention of A1094 in serum over 120 min. (f) Serum protein loading capacity of A1094. (g, h) Photothermal conversion properties of A1094, Blank = aqueous solution (0.25% DMSO). (i) Illustration drawing of the preparation of A1094 injection. (j) Comparison of absorption intensities between A1094 and Au nanorods at the concentration of 0.05 mg/mL. (k) PA intensity of A1094 in a series of concentrations (1.0, 0.5, 0.25, 0.125, and 0.0625 mg/mL) in aqueous solutions (0.25% DMSO). (l) PA intensity of Au nanorods in a series of concentrations (1.0, 0.5, 0.25, 0.125, and 0.0625 mg/mL).

good stability, which is conducive to further study *in vivo*. Furthermore, after the preparation of A1094 injection, it could be stored for 24 h without change.

Photothermal and PAI properties of A1094

Time-temperature curves and photothermal images showed that the photothermal efficiency was linearly dependent on the concentration of A1094 (Figures 1g, 1h). At 172 μM , there was an increase in temperature by 20 °C after irradiation (1 W/cm², 5 min), whereas the temperature of the blank (ultrapure water with 0.25% DMSO) increased by only 6 °C. Besides excellent photothermal conversion efficacy, the absorption intensity of A1094 in 0.25% DMSO aqueous solution measured at 8 different time points over a course of 140 min was basically unchanged, indicating the photothermal stability of A1094 (Figure 1a). Quantitative analysis of the PA signal showed that there was a linear relationship between PA signal and the concentration of A1094. In addition, the PA signal of A1094 was superior to that of the Au nanorods at the same mass concentration, an observation which highlights the potential of A1094 for use in PAI (Figures 1k, 1l).

PAI of murine ears with and without acute inflammation

To evaluate the effect of A1094 injection as contrast agent *in vivo*, it was intravenously injected to murine ear vessels. As strong as 3.25 times PA signal was observed in acutely inflamed murine ear vessels, compared with that in normal vessels

(Figure 2a–d). Local blood vessel dilation with little acute exudate was clearly observed in inflamed ears. When Au nanorods were injected in inflammation and control vessels instead, 58% enhancement of PA signal was found in the former case. This indicated the potentially at least comparable sensitivity imparted by the use of A1094 in angiography (Figure 2e–h).

PAI of murine livers

The PA signal intensity was significantly enhanced during the period 0–2 min after i.v. injection, indicating that A1094 possessed the ability to provide enough blood pool imaging contrast. At 2–50 min period, the PA signal drops rapidly from the peak. Moreover, the PA signal essentially disappeared at 50 min post-injection, which was cleared by 74.2% after 3 h, indicating that A1094 was highly conducive to liver clearance (Figure 3a). The rapid clearance may also be related to its low plasma protein binding rate (15.1%, Figure 1f). Since liver is the main metabolic organ of lipophilic small molecules, fast clearance of absorber would not only reduce background interference but also relieve liver burden. In contrast, after the i.v. injection of Au nanorods, the PA signal increased slowly and reached its peak value after 10 min. The PA signal also decreased slowly, which was cleared by 43.1% after 3 h, and was still perceptible on the seventh day, indicating poor hepatic metabolism of Au nanorods (Figure 3b). Au nanorods were easily ingested by the liver and not easily degraded after ingestion. However, A1094 was easily degraded in liver, which

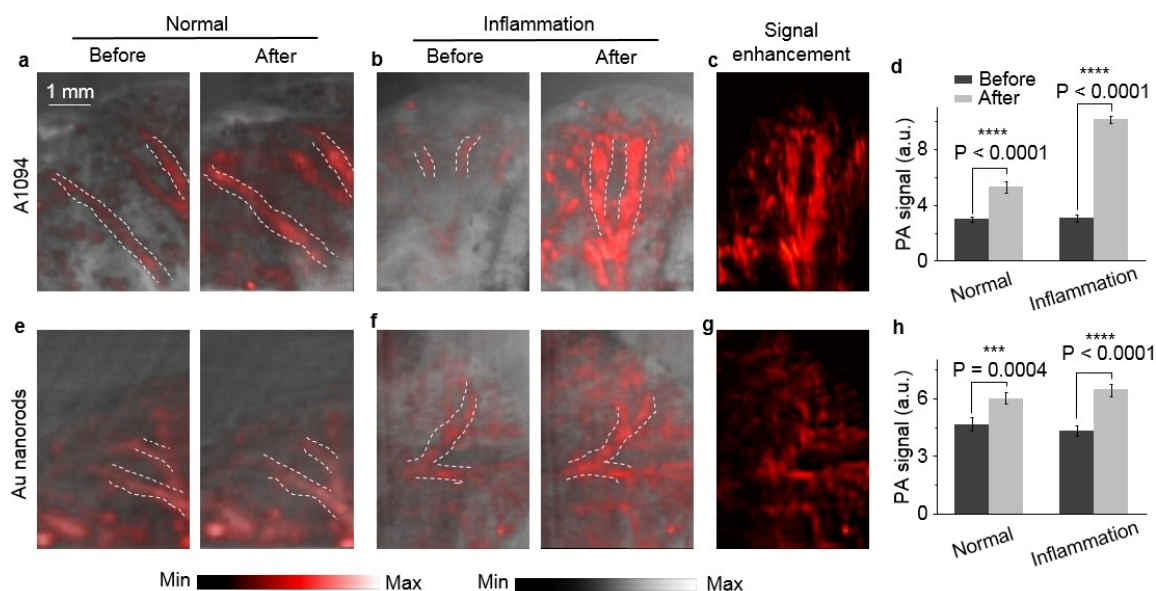


Figure 2. PAI of murine ears with A1094 and Au nanorods. (a) PAI of murine ears after i.v. injection of A1094 under 970 nm laser irradiation. (b) PAI of murine ears with inflammation after i.v. injection of A1094 under 970 nm laser irradiation. (c) Increased PA signal in the inflammation ear after injection of A1094 solution. (d) Corresponding PA intensity of (a) and (b). (e) PAI of murine ears after i.v. injection of Au nanorods under 970 nm laser irradiation. (f) PAI of murine ears with inflammation after i.v. injection of Au nanorods under 970 nm laser irradiation. (g) Increased PA signal in the inflammation ear after injection of Au nanorods. (h) Corresponding PA intensity of (e) and (f).

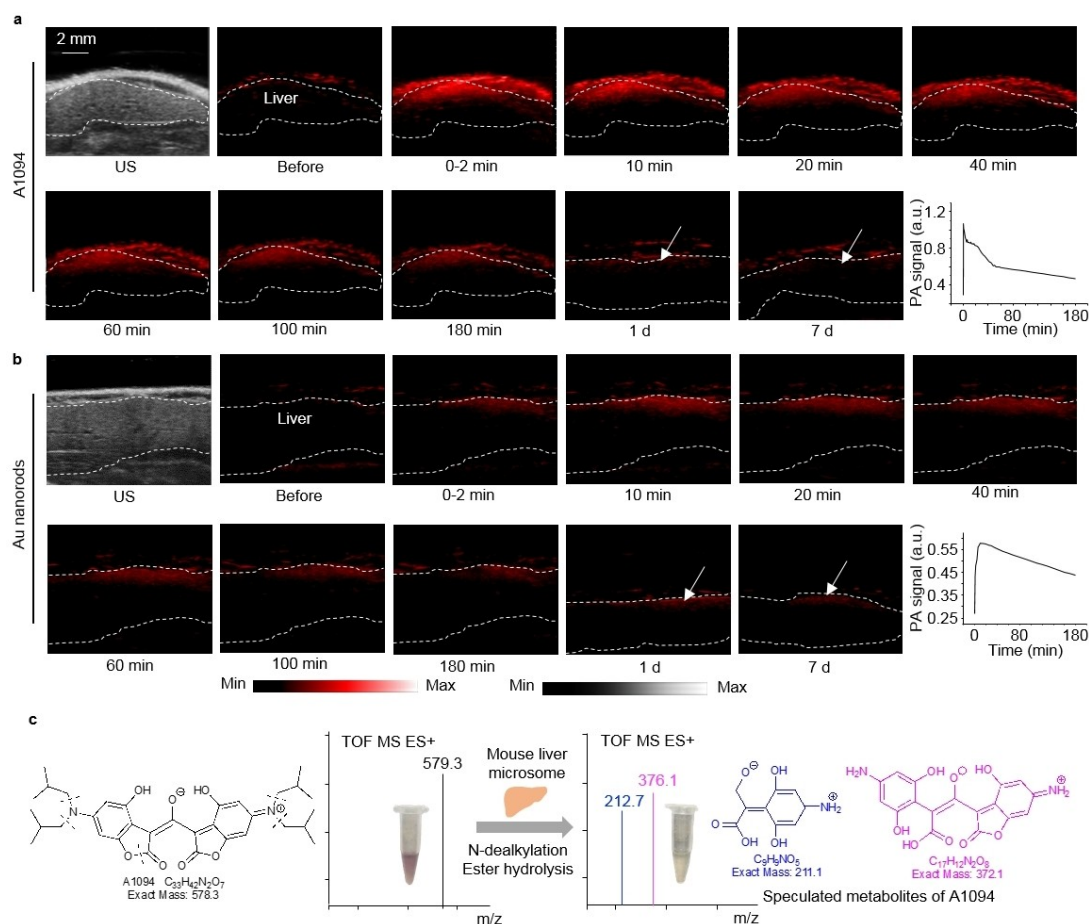


Figure 3. Metabolism of A1094 *in vivo* and *in vitro*. (a) PAI of murine livers after i.v. injection of A1094 and corresponding PA signal value. (b) PAI of murine livers after i.v. injection of Au nanorods and corresponding PA signal value. (c) Structure and mass spectrum of A1094 and its metabolites after metabolism by murine liver microsomes *in vitro*.

lead to rapid elimination of PA signal in liver compared with Au nanorods.

Evaluation of A1094 metabolites in mouse liver microsome

After incubation with mouse liver microsomes *in vitro*, the MS molecular peak corresponding to A1094 completely disappeared from the MS spectra. Two new peaks appeared, with MS (ESI) m/z values of 212.7 and 376.1 ($[M+H]^+$). Based on the structure of A1094, N-dealkylation and lipid hydrolysis were considered to be the modes of A1094 metabolism (Figure 3c). The metabolites were water-soluble and easily discharged from the body, so they showed few toxic side effects. In addition, the absorption intensity at 1094 nm was weakened after liver hydrolysis, corresponding to the rapidly decreasing liver PA signal value during 2–50 min.

Existing NIR-II PA contrast agents are inorganic nanomaterials, which are usually not conducive to metabolism *in vivo*. However, PAI in murine livers showed that A1094 was more conducive to liver clearance than Au nanorods, suggesting that A1094 might be a promising candidate for clinical use.

Biocompatibility and biosafety of A1094 injections.

Even at concentrations of up to 200 μ M, the survival of N₂a cells remained high (Figure 4a), indicating that A1094 was significantly safe and biocompatible. This observation laid the foundation for further applications *in vivo*.

When the main organs of the mice were collected for H&E staining, tissue morphology revealed A1094 injection to be safe for use (Figure 4b), as no obvious damage was observed. There was no significant change in serum chemistry (Figure 4h–k) or whole blood parameters (Figures 4d–g, S3). During long-term toxicity testing, the skin colour and eyes of the mice were normal, no abnormal phenomena were found, and no death occurred, further indicating that the preparation had good biocompatibility (Figure 4c).

Conclusion

In summary, an injection of the small-molecular croconaine absorber A1094 were prepared for NIR-II photoacoustic imaging. In the NIR-II window, A1094 possessed an absorption

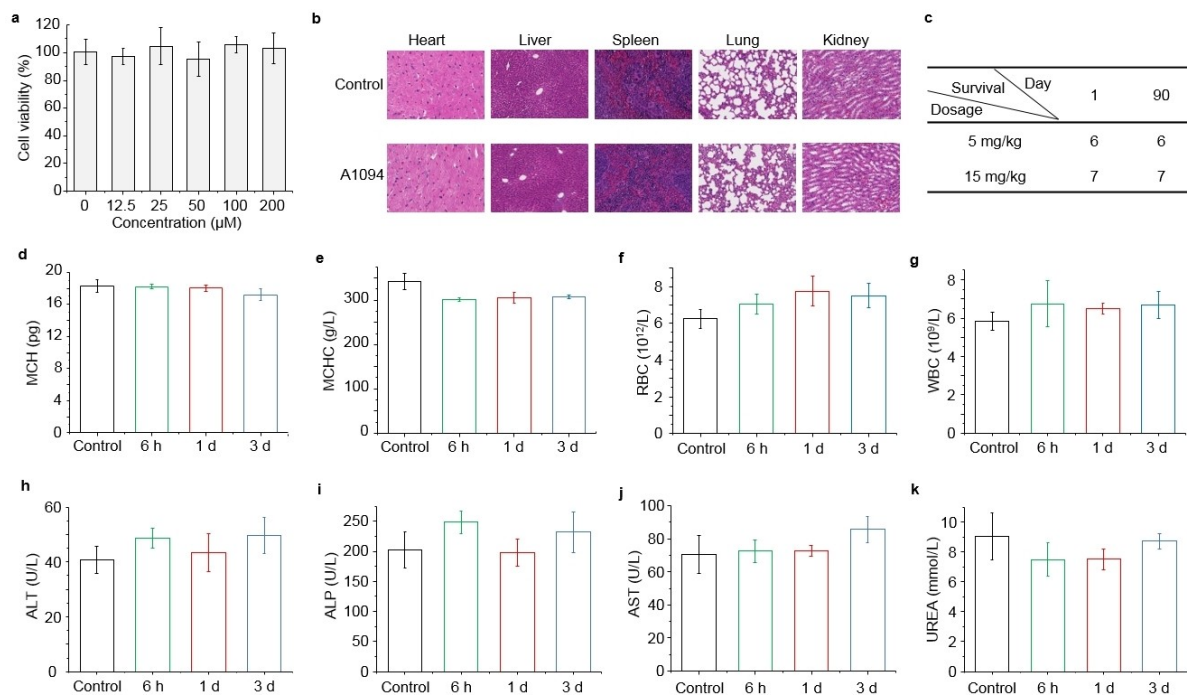


Figure 4. Biocompatibility and toxicity of A1094. (a) Cell viability of N₂a cells after treatment with different concentrations of A1094. (b) H&E staining of major organs from mice administered A1094 for 3 days (15 mg/kg, n=3). (c) Amount of survival mice after 90 days. (d–g) Haematological analysis of mice treated with PBS or A1094. MCH: mean corpuscular hemoglobin; MCHC: mean corpuscular hemoglobin concentration; RBC: red blood cell; WBC: white blood cell. (h–k) Serum chemistry of mice treated with PBS or A1094. ALT: alanine transaminase; ALP: alkaline phosphatase; AST: aspartate transaminase; UREA: blood urea nitrogen.

efficiency comparable to that of the Au nanorods, and produced effective NIR-II imaging. With deeper penetration into the NIR-II window, the PAI of inflamed murine ears showed a significantly enhanced PA signal and a rich contrast after intravenous injection of A1094, and the images clearly showed dilated vessels and blood exudate. Moreover, A1094 exhibited good pH stability, metal ion stability, oxidation-reduction stability, photothermal performance, and PA signal strength, which are considerable advantages for use as a PAI contrast agent.

N-dealkylation and lipid hydrolysis were identified as the main metabolic pathways of A1094. Rapid hepatic clearance was observed after the imaging window, indicating a high level of biosafety and a reduced metabolic burden. Therefore, A1094 may be more easily approved for clinical use than other imaging agents. Our tests of A1094 were repeatable, which is difficult to achieve in nanomaterial investigations. The method of purity identification was simple and easily reproducible.

Due to the limited water solubility of A1094, its structure should be modified to improve its water solubility in follow-up studies, making it more suitable for application *in vivo*. In addition, some targeted modifications could be made to make it specifically bind to biomarkers *in vivo*, an approach which is valuable for the diagnosis of disease.

Experimental Section

A1094 was obtained using a modified version of a previously reported protocol,^[27] and characterized by ¹H, ¹³C nuclear magnetic resonance (NMR) spectroscopies and mass spectrometry (MS).

Stabilities of A1094

Solubility of A1094 in different solvents. Equal amounts of A1094 (2.0 mg, 3.5 μmol) were added to each of several clean tubes. Then 0.5 mL each of methanol, DMSO, dichloromethane, acetonitrile, cyclohexane, n-hexane, and ethanol were added to the tubes, and the complete dissolution of A1094 after vortex vibration was observed. Meanwhile, different amounts of A1094 were placed in a clean tube, 50 μL DMSO was added, and the volume made up to 20 mL with ultrapure water; this produced a 99.75% aqueous solution with 0.25% DMSO. The solubility of A1094 in aqueous solution was observed to be up to 0.5 mg/mL (0.86 mM).

Stability of A1094 in different solvents. The absorption spectra of A1094 at intervals of 30 or 40 min in each of the different solvents (methanol, DMSO, dichloromethane, acetonitrile and ethanol) were recorded.

pH stability. A1094 was dissolved in aqueous solutions (0.25% DMSO, 99.75% aqueous solution: v/v, 25 μg/mL, 43.3 nmol/mL) with different pH values (from 2 to 12).

Stability in the presence of different metals. A1094 was dissolved in aqueous solutions (0.25% DMSO, 50 μg/mL, 86.6 nmol/mL) and various metal ions (1.0 mM K⁺, Na⁺, Ca²⁺, and Mg²⁺; 25 μM Ba²⁺, Co²⁺, Fe³⁺, Mn²⁺, Ni²⁺, Pb²⁺, Al³⁺, Fe²⁺, Cu⁺, and Cu²⁺) were added respectively to the solutions. The absorption spectra were measured after 2 h incubation.

Stability in the presence of H₂O₂ and glutathione. A1094 was dissolved in aqueous solutions (0.25% DMSO, 50 µg/mL, 86.6 nmol/mL). H₂O₂ (100 µM) and glutathione (100 µM) were added respectively to the solutions. The absorption spectra were measured after 2 h incubation.

Stability in serum. A1094 was dissolved in aqueous solutions (0.25% DMSO, 50 µg/mL, 86.6 nmol/mL) and 200 µL of the solution was added to 2 mL of serum. The absorption spectra were recorded at intervals of 30 min over a course of 120 min.

Determination of the plasma protein binding rate

Specified amounts of A1094 (12.5, 25, and 50 µg/mL) were dissolved in 50 µL of DMSO, 950 µL of foetal bovine serum (FBS) was added, and the solutions were mixed using a vortex mixer. The samples were incubated at a constant temperature of 37 °C in a water bath for 60 min. The incubated solutions were removed and placed on ice, and the temperature was maintained at approximately 4 °C. Next, 500 µL of each solution was transferred to an ultrafiltration tube, placed in a low-temperature centrifuge, and centrifuged at 4 °C at 14000×g for 20 min to obtain ultrafiltration solutions. The absorption spectra of the incubated and ultrafiltered solutions were determined. The binding rate of plasma proteins and the standard absorption-mass curve of A1094 was calculated using formula (1).

$$\text{Plasma protein binding rate (\%)} = \left[\frac{C_{(\text{incubation solution})} - C_{(\text{ultrafiltration solution})}}{C_{(\text{incubation solution})}} \right] \times 100 \quad (1)$$

$C_{(\text{incubation solution})}$ represents the mass concentration (µg/mL) of A1094 in the incubation solution before ultrafiltration, and $C_{(\text{ultrafiltration solution})}$ represents the mass concentration (µg/mL) of A1094 in the ultrafiltration solution.

Preparation and quality control of the A1094 injection

Preparation of the A1094 injection. Before i.v. injection, 1.0 mg A1094 was dissolved in 20 µL DMSO. Then, 50 µL of Tween 80, a commonly used solubilizer, and 930 µL of saline were added and mixed using ultrasound to prepare a 1.0 mL solution, i.e., 1.0 mg/mL A1094 injection.

Quality control of the A1094 injection. The A1094 injection – with a pH between 5.0–8.0 – was a clear solution, and exhibited a main peak at 1094 nm in the UV spectra. In order to ensure the sterility of the injection, all A1094 injections were filtered through 0.22-µm filter membranes before use. In addition, to ensure a uniform effect of the injection dose, 100 µL was decided as the injection dose per mouse throughout the whole experimental process.

Preparation of Au nanorod injection. Aqueous solutions of Au nanorods with a 1125 nm absorption at the same mass concentration gradient were prepared, and the PA signals were measured at 1200 nm and 970 nm.

Photothermal and PAI properties. To test the photothermal effects, A1094 in aqueous solution (10.8, 21.5, 43, 86, 172 µM) was exposed to a 980 nm laser (1 W/cm² for 6 min). During laser irradiation, the temperature was continuously monitored using a charge-coupled device camera. To study photothermal stability, the absorption spectrum of A1094 was evaluated before and after treatment with laser irradiation. We recorded the absorption spectrum of A1094 at intervals of 10 or 20 min over the course of 140 min. A1094 solutions with concentrations of 1.0, 0.5, 0.25,

0.125, and 0.0625 mg/mL were prepared. The PA signals were measured at 1200 nm and 970 nm.

PAI of murine ears with and without acute inflammation

All of the animals used in the experiment were provided by the Experimental Animal Center of Xiamen University. ICR mice were 4–5 weeks old, weighed 18–22 g, and were male. The animal experiments were conducted in accordance with the Guidelines for Laboratory Animal Use and Care approved by the Xiamen University Animal Care and Use Committee.

Establishment of acute ear inflammation model in mice. 30 µL xylene was daubed on the upper and lower sides of the right auricle of ICR mice for 20 min to induce acute ear swelling as a model of inflammation.

PAI of murine ears with and without acute inflammation. To explore the *in vivo* PAI potential of A1094, PAI of murine ears with and without acute inflammation was conducted. Firstly, the PAI of normal murine ears were scanned, and PAI signals were collected immediately after i.v. injection of A1094. Moreover, the PAI of the inflamed murine ears were scanned, and PAI signals were collected immediately after i.v. injection of Au nanorods. The PAI abilities of A1094 and Au nanorods were compared *in vivo* by injecting each agent into mice without acute inflammation.

Evaluation of metabolites of A1094

PAI of clearance of A1094 from murine livers *in vivo*. After an intravenous injection of A1094, the dynamic processes of liver metabolism were visualised, and the PA signal of the A1094 was quantified, to measure the metabolic clearance rate.

Preparation of murine liver microsomes. After fasting for 16 h, the mice were sacrificed using cervical vertebral dislocation, and a laparotomy was performed. Then, normal saline cooled in an ice bath was aspirated with a syringe, injected into the liver through the thoracic artery or portal vein, and perfused until the liver turned white, indicating that the blood in the liver had been removed. The liver microsomes were prepared using differential centrifugation. First, the liver tissue was weighed, cut into pieces, and washed repeatedly with 0.1 mol/L potassium phosphate buffer (pH 7.4). Then, the above buffer was added at a ratio of 1:4 (w/v), and the tissue was placed in an ice bath with a glass homogeniser. The supernatant was centrifuged at 9000×g for 20 min at 4 °C and then at 100 000×g for 60 min. The liver microsomes were resuspended with buffer containing 20% glycerol and then placed in a refrigerator at –80 °C on standby.

Metabolite analysis. 100 µL diluent of the murine liver microsomes was taken and 200 µL of an NADPH coenzyme regeneration system (0.5 mmol/L NADP⁺, 5 mmol/L G-6-P, 2 unit/mL G-6-PDH, 6 mmol/L magnesium chloride), which was freshly prepared and pre-aerated for 1 min, was added and mixed well to yield the pre-incubation solution. The pre-incubation solution was placed in a 37 °C water bath and shaken for 3 min. Next, 100 µL of the 80 µmol/L A1094 solution was added to initiate the incubation reaction (the final concentration of A1094 was 20 µmol/L). Lastly, 200 µL of cold acetonitrile solution was added to the incubation tube, which was then quickly immersed in an ice bath to stop the reaction.

Biocompatibility test

A1094 cytotoxicity assessment. Mouse neuroblastoma N₂a cells were seeded into 96-well plates at a concentration of 5 × 10³ cells/

well and cultured for 24 h. Then, N₂a cells were treated with different concentrations of A1094 (0, 12.5, 25, 50, 100 and 200 μM). After 12 h, the viability of N₂a cells was evaluated by standard CCK-8 test.

Haematoxylin and eosin (H&E) staining. After i.v. injection of A1094 at 15 mg/kg for 3 days, the major organs (heart, liver, spleen, lung, kidney) of the mice were collected for H&E staining to assess the cytotoxicity of A1094.

Haematological analysis. Samples of 500 μL whole blood were collected before and 6 h, 1 d and 3 d after i.v. injection of A1094 at 15 mg/kg. The blood was placed at room temperature for 1 h, at 4 °C for 3–4 h, and then centrifuged at 3000 r/min for 10 min. The supernatant was stored at 4 °C for serum chemical analysis.

Serum chemistry. About 50 μL of mice blood was collected before and 6 h, 1 d and 3 d post i.v. injection of A1094, and placed in anticoagulant tubes containing heparin sodium. The venous blood was fully mixed with anticoagulant and stored at 4 °C for haematological analysis. Refrigerated samples were kept at room temperature for 30 min and remixed before analysis.

Long-term toxicity test. Male ICR mice (4–5 weeks old) were fed under conditions of 12 h/12 h light/dark cycle for a week. The mice were injected with 5 mg/kg or 15 mg/kg A1094 once per week for three consecutive weeks. The skin, eyes and activity of mice were observed continuously, and the survival rate was recorded.

Acknowledgements

This study was financially supported by the National Natural Science Foundation of China (81971674), Science Fund for Distinguished Young Scholars of Fujian Province (2019J06006), Fundamental Research Funds for the Central Universities (20720180050), and the Scientific Research Foundation of State Key Laboratory of Molecular Vaccinology and Molecular Diagnostics (2016ZY002).

Conflict of Interest

The authors declare no conflict of interest.

Keywords: croconaine absorber · small molecule · photoacoustic imaging · optical contrast agent · the second near-infrared window

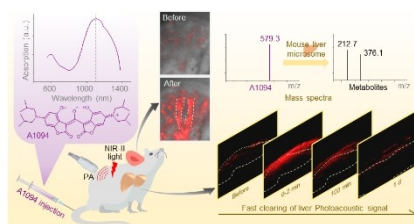
[1] P. K. Upputuri, M. Pramanik, *J. Biomed. Opt.* **2019**, *24*, 1–20.

- [2] P. Beard, *Interface Focus* **2011**, *1*, 602–631.
 [3] Kenry, Y. Duan, B. Liu, *Adv. Mater.* **2018**, *30*, e1802394.
 [4] G. Hong, S. Diao, J. Chang, A. L. Antaris, C. Chen, B. Zhang, S. Zhao, D. N. Atochin, P. L. Huang, K. I. Andreasson, C. J. Kuo, H. Dai, *Nat. Photonics* **2014**, *8*, 723–730.
 [5] A. L. Antaris, H. Chen, K. Cheng, Y. Sun, G. Hong, C. Qu, S. Diao, Z. Deng, X. Hu, B. Zhang, X. Zhang, O. K. Yaghi, Z. R. Alamparambil, X. Hong, Z. Cheng, H. Dai, *Nat. Mater.* **2016**, *15*, 235.
 [6] V. Ntziachristos, *Nat. Methods* **2010**, *7*, 603–614.
 [7] J. E. Lemaster, J. V. Jokerst, *Wires Nanomed. Nanobi.* **2017**, *9*, e1404.
 [8] H. H. Liu, X. Y. Wang, Y. F. Huang, H. H. Li, C. Y. Peng, H. Z. Yang, J. D. Li, H. W. Hong, Z. Lei, X. F. Zhang, Z. J. Li, *ACS Appl. Mater. Interfaces* **2019**, *11*, 30511–30517.
 [9] G. Ku, M. Zhou, S. Song, Q. Huang, J. Hazle, C. Li, *ACS Nano* **2012**, *6*, 7489–7496.
 [10] Y. Zhang, G. Hong, Y. Zhang, G. Chen, F. Li, H. Dai, Q. Wang, *ACS Nano* **2012**, *6*, 3695–3702.
 [11] R. Subha, V. Nalla, J. H. Yu, S. W. Jun, K. Shin, T. Hyeon, C. Vijayan, W. Ji, *J. Phys. Chem. C* **2013**, *117*, 20905–20911.
 [12] K. Welscher, S. P. Sherlock, H. Dai, *Proc. Natl. Acad. Sci. USA* **2011**, *108*, 8943–8948.
 [13] Y. Jiang, P. K. Upputuri, C. Xie, Y. Lyu, L. Zhang, Q. Xiong, M. Pramanik, K. Pu, *Nano Lett.* **2017**, *17*, 4964–4969.
 [14] Z. Zha, Z. Deng, Y. Li, C. Li, J. Wang, S. Wang, E. Qu, Z. Dai, *Nanoscale* **2013**, *5*, 4462–4467.
 [15] D. Miranda, H. Huang, H. Kang, Y. Zhan, D. Wang, Y. Zhou, J. Geng, H. I. Kilian, W. Stiles, A. Razi, J. Ortega, J. Xia, H. S. Choi, J. F. Lovell, *Theranostics* **2019**, *9*, 381–390.
 [16] C. Sun, B. Li, M. Zhao, S. Wang, Z. Lei, L. Lu, H. Zhang, L. Feng, C. Dou, D. Yin, H. Xu, Y. Cheng, F. Zhang, *J. Am. Chem. Soc.* **2019**, *141*, 19221–19225.
 [17] A. V. Dsouza, H. Lin, E. R. Henderson, K. S. Samkoe, B. W. Pogue, *J. Biomed. Opt.* **2016**, *21*, 80901.
 [18] K. Cheng, H. Chen, C. H. Jenkins, G. Zhang, W. Zhao, Z. Zhang, F. Han, J. Fung, M. Yang, Y. Jiang, L. Xing, Z. Cheng, *ACS Nano* **2017**, *11*, 12276–12291.
 [19] Q. Fan, K. Cheng, Z. Yang, R. Zhang, M. Yang, X. Hu, X. Ma, L. Bu, X. Lu, X. Xiong, W. Huang, H. Zhao, Z. Cheng, *Adv. Mater.* **2015**, *27*, 843–847.
 [20] M. Tian, S. Tatsuura, M. Furuki, Y. Sato, I. Iwasa, L. S. Pu, *J. Am. Chem. Soc.* **2003**, *125*, 348–349.
 [21] H. Langhals, *Angew. Chem. Int. Ed.* **2003**, *42*, 4286–4288; *Angew. Chem.* **2003**, *115*, 4422–4424.
 [22] S. Zhang, X. Yang, X. Wen, S. Ding, A. Wang, *Chin. J. Org. Chem.* **2014**, *34*, 223–229.
 [23] Y. Liu, Y. Yang, M. Sun, M. Cui, Y. Fu, Y. Lin, Z. Li, L. Nie, *Chem. Sci.* **2017**, *8*, 2710–2716.
 [24] D. E. Lynch, D. G. Hamilton, *Eur. J. Org. Chem.* **2017**, *2017*, 3897–3911.
 [25] K. Srinivas, C. Prabhakar, C. L. Devi, K. Yesudas, K. Bhanuprakash, V. J. Rao, *J. Phys. Chem. A* **2007**, *111*, 3378–3386.
 [26] P. K. Upputuri, M. Pramanik, *J. Biomed. Opt.* **2019**, *24*(4), 040901.
 [27] Y. Liu, H. Liu, H. Yan, Y. Liu, J. Zhang, W. Shan, P. Lai, H. Li, L. Ren, Z. Li, L. Nie, *Adv. Sci.* **2019**, *6*, 1801615.

Manuscript received: February 22, 2021
 Revised manuscript received: April 18, 2021
 Accepted manuscript online: April 20, 2021
 Version of record online: ■■■, ■■■■

FULL PAPERS

Because most current NIR-II imaging agents are poorly metabolised *in vivo*, the small-molecule absorber A1094 is considered a photoacoustic imaging contrast agent *in vivo*. The imaging ability of A1094 is similar to that of the standard Au nanorod agent, and A1094 possesses the stability, safety, and rapid background clearance *in vivo* which are required of optical probes for potential clinical NIR-II photoacoustic imaging. Comprehensive preclinical evaluation and potential application of A1094 injection in basic blood pool imaging is presented for the first time.



Y. Huang, H. Liu, X. Chen, Y. Zhang, X. Zhao, W. Huang, Z. Mou, C. Wang, K. Zhang, Dr. Z. Li*

1 – 8

Small-Molecule Absorber A1094 as a Stable and Fast-Clearing NIR-II Imaging Agent

